Dynamic Conformational Behavior in Stable Pentaorganosilicates

van der Boon, L.J.P.; Hendriks, J.H.; Roolvink, D.; O'Kennedy, S.J.; Lutz, M.; Slootweg, J.C.; Ehlers, A.W.; Lammertsma, K.

DOI
10.1002/ejic.201900641

Publication date
2019

Document Version
Final published version

Published in
European Journal of Inorganic Chemistry

ChemPubSoc Europe

DOI: 10.1002/ejic.201900641

EurJIC European Journal of Inorganic Chemistry

Full Paper

Dynamic Silicates

Dynamic Conformational Behavior in Stable Pentaorganosilicates

Leon J. P. van der Boon,[a] Jesper H. Hendriks,[a] Danny Roolvink,[a] Sean J. O'Kennedy,[b] Martin Lutz,[c] J. Chris Slootweg,[a,d] Andreas W. Ehlers,*[a,d,e] and Koop Lammertsma*[a,e]

Abstract: Silicates with five organic groups are conformationally dynamic even with two bidentate ligands. Symmetry breaking by incorporating a single nitrogen or phosphorus atom provides insight into their dynamic behavior. N-containing silicates with bidentate 2-phenylpyridine, biphenyl, and a Me (**8**), Et (**9**) or Ph (**10**) ligand were studied comprehensively by NMR spectroscopy and DFT theory to reveal two isoenergetic conformers with a barrier of ca. 10 kcal mol^{-1}. P-containing silicate **14** with bidentate triphenylphosphane, biphenyl, and Me ligands is subject to multiple Berry pseudorotations, turnstile rotations, and conformational flexibility of the P-center. The stability increased by masking the P-center with a BH_3 group (**16**). DFT and NMR modeling reveal two isoenergetic conformers for **16** with a barrier of ca. 19 kcal·mol^{-1} for a complex interconversion pathway. This barrier bodes well for the design of configurationally stable chiral-at-metal transition metal catalysts.

Introduction

Silicates with five organic substituents are remarkably stable compounds.[1–3] Their stabilization is typically attributed to the electron withdrawing nature of the organic ligands or the coordinating heteroatoms,[4] which are often oxygen and/or nitrogen atoms (e.g., **1**; Scheme 1), but silicates carrying only carbon groups can also be quite stable (m.p. > 150 °C), provided the presence of two aromatic bidentate ligands as in **2a**.[5–7] For example, two biphenyl ligands give so much stability that the fifth group occupies an equatorial position even if it is a fluorine atom, thereby seemingly violating the notion of apicophilicity.[8]

In our recent studies on all-carbon pentaorganosilicates we focused on controlling the dynamic stereomutations that result from Berry pseudorotations.[9] Similar permutations have also been observed in silicates containing a heteroatom, like **4**.[10] By using adequately sized bidentate ligands, such as two 2-(phenyl)-naphthyl units (**2c**),[11] selected pseudorotations can be hindered to enable the isolation of chiral silicates in spite of the dynamic nature of the enantiomers. Silicates like **2c** but also phosphoranes like **3**[12] are chiral at the central atom and do not require asymmetric ligands as in, e.g., **1**.

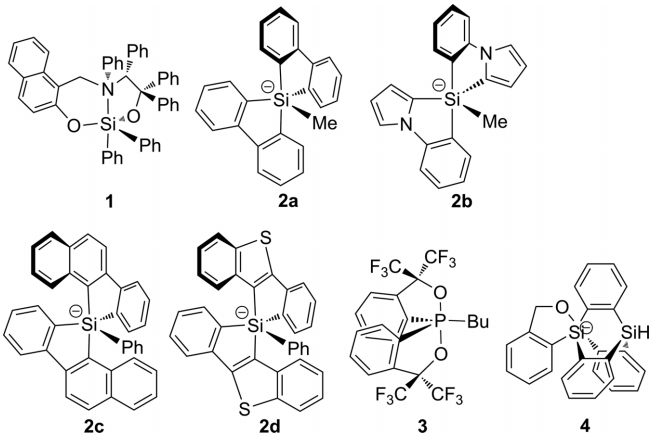

Scheme 1. Pentacoordinate species subject to Berry pseudorotations.

To advance the access to and to enhance the insight into manipulating the dynamics of pentaorganosilicates that are chiral-at-silicon it is desirable to expand the scope of bidentate ligands. We opted for simple aromatic ones, because these can be extended by, e.g., catenated phenyl groups or aromatic substituents to increase congestion if needed. Earlier, we reported on silicates carrying two N-phenylpyrroles[9] (**2b**) and two 2-(phenyl)benzo[*b*]-thiophenes (**2d**),[11] but whereas their conformers may be detectable by NMR spectroscopy, DFT calculations revealed the chelation of the five-membered pyrrole and thiophene rings to be less suited for inhibiting Berry pseudorotations than the six-membered phenyl ring (**2c**).

[a] *Faculty of Sciences, Vrije Universiteit Amsterdam, De Boelelaan 1083, 1081 HV Amsterdam, The Netherlands*
E-mail: a.w.ehlers@uva.nl
k.lammertsma@vu.nl
[b] *Department of Chemistry and Polymer Science, Stellenbosch University, Private Bag X1, Matieland, 7602, South Africa*
[c] *Crystal and Structural Chemistry, Bijvoet Center for Biomolecular Research, Utrecht University, Padualaan 8 3584 Utrecht, The Netherlands*
[d] *Van 't Hoff Institute for Molecular Sciences, University of Amsterdam, Science Park 904, 1090 GD Amsterdam, The Netherlands*
[e] *Department of Chemistry, Science Faculty, University of Johannesburg, PO Box 254, Auckland Park, Johannesburg, South Africa*
Supporting information and ORCID(s) from the author(s) for this article are available on the WWW under https://doi.org/10.1002/ejic.201900641.

In this work, we report on two novel pentaorganosilicate templates that feature *one six*-membered heterocyclic ring with either a nitrogen or a phosphorus atom in only *one* of the bidentate ligands. Here we present their syntheses and describe their complex dynamic properties using NMR spectroscopy and DFT calculations. These analyses seek to provide criteria for controlling the chirality of silicates and by inference how to control the dynamics in chiral-at-metal catalysts.[13–17]

Results and Discussion

We start with the silicate of which one of the bidentate ligands contains a single pyridine ring. This silicate represents the closest N-hetero analogue to **2**.

N-containing silicates 8–11 – experimental. As starting material we used dichlorobiphenylsilane **5**, which can be obtained from dilithiated 2,2′-dibromobiphenyl and $SiCl_4$. The Li_2-salt is soluble in Et_2O, reacts with $SiCl_4$ in yields up to 71 %, but requires a product distillation step.[18,19] A THF suspension reacts slower, but gives a higher yield (86 %) and requires only product purification by washing with *n*-pentane. Reaction of **5** with the Li_2-salt of 3-bromo-2-(2-bromophenyl)-pyridine (**6**) afforded the single pyridine containing spirosilane **7** in 52 % isolated yield (Scheme 2).[20] Treatment of the silane with MeLi, EtLi, and PhLi gave the desired silicates **8**, **9**, and **10**, respectively. The ^{29}Si-NMR spectra show the characteristic high field resonance for each silicate (**8** –107.2; **9** –101.6; **10** –102.2 ppm). All have ^{1}H NMR spectra as expected as do the exact mass spectroscopic measurements. The melting points of the silicates are noteworthy lower than that for **2a** (**8** 47.2; **9** 77.6; **10** 107.3 °C (dec.; **2a**, nBu_4N^+ counterion, 180 °C).

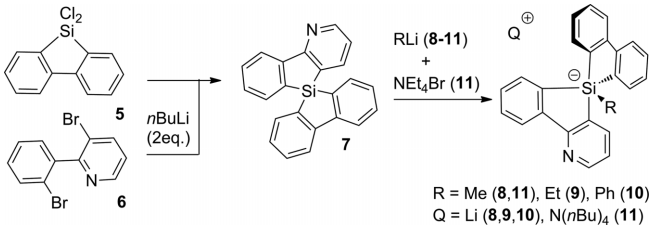

Scheme 2. Synthesis of pyridine bearing pentaorganosilicates.

A single-crystal X-ray structure confirms the identity of the phenyl derivative **10** (Figure 1). Its molecular structure features a biphenyl and a phenylpyridine ligand in a screw-like fashion that underlies the inherent chiral property of this silicate; **10** is, of course, present as a dynamically racemizing enantiomeric pair. The phenyl substituent is located in the equatorial position of the trigonal bipyramid. Its rather small torsion angle of 58.1(3)° with the axial Si–C bond is likely due to both steric repulsion and the unfavorable π-interaction of the phenyl ring with the axial bond.[4] The Li^+ counterion is coordinated to the pyridine nitrogen atom (d_{NLi} 2.066(5) Å) and is further stabilized by three THF solvent molecules. This behavior differs from non-coordinating silicates like **2a** that crystallize with a tetra-THF coordinated Li^+ ion.

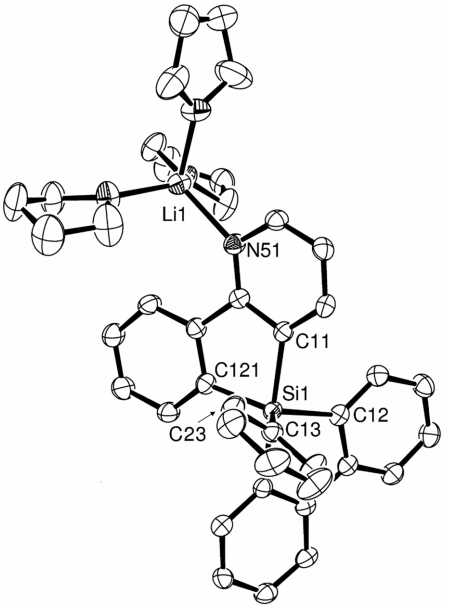

Figure 1. Molecular structure **10** in the crystal (ellipsoids are set at 50 % probability; hydrogen atoms are omitted for clarity). Only the major component of the disordered THF groups is shown. The structure crystallizes as a racemic mixture of enantiomerically pure crystals in space group $P2_1$. Selected bond lengths [Å], angles and torsion angles [°]: Si1–C12 1.935(3), Si1–C11 2.016(3), Si1–C13 1.926(3), Si1-C121 1.940(3), N51–Li1 2.066(5), C13–Si1–C121 117.63 (12), C12–Si1–C121 122.89 (12), C11–Si1–C12 94.93 (11), C11–Si1–C13 88.72 (11), C23–C13–Si1–C11 58.1 (3).

Pyridine silicates **8–10** are highly dynamic. Broad resonances are observed at room temperature in both the aromatic and aliphatic regions of the ^{1}H NMR spectra ([D_8]THF). Neither are all carbon resonances resolved in the ^{13}C NMR spectra. Lowering the temperature gradually to –80 °C has a significant effect as is illustrated for the ^{1}H NMR spectra of **8** in Figure 2 (see SI for more details). At –80 °C two resonances (δ = 0.247 and 0.268 ppm) are observed for the Me group with the major one being broadened, possibly resulting in overlap of two signals as shown by deconvolution (see SI) and thereby preventing a more detailed analysis.

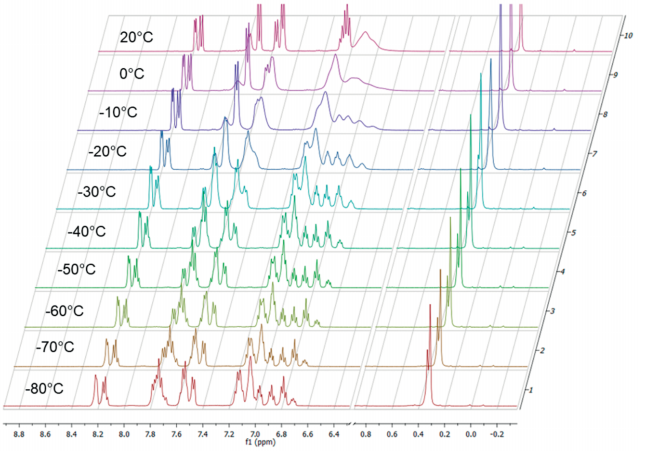

Figure 2. ^{1}H NMR of **8** measured at intervals from 20 to –80 °C.

We presume the Me resonances to originate from two near-isoenergetic conformers of **8** that are in rapid equilibrium with

a coalescence temperature of ca. –10 to –20 °C. The aromatic region shows likewise behavior in the same temperature range. This dynamic behavior is reminiscent to that reported for bispyrrole-phenyl silicate **2b** (coalescence at ca. –12 °C, $\Delta G^{\ddagger}$= 15.5 kcal·mol^{-1}), which has been attributed to Berry pseudorotation between near-isoenergetic conformers. The dynamic exchange for pyridine silicate **8** appears to occur at a slightly lower temperature and thus a little faster than for silicate **2b** assuming similar chemical shift differences, suggesting somewhat smaller conversion barriers between the near-isoenergetic conformers of **8**. To obtain more insight into the dynamic behavior we resorted to DFT calculations.

N-Containing Silicates 8 and 10 – Computational

A survey for **8** and **10** was conducted at the B3LYP-D3/6-311++G(2p,d)// B3LYP/6-31G(d) level. Figure 3 shows the two pairs of enantiomeric conformations (**Δ/Λ8a** and **Δ/Λ8b**) and the transition structures connecting them. The minimum energy structure **8a** has the pyridine ring in an axial position of a trigonal bipyramid with the methyl group occupying an equatorial position. With a barrier of 10.9 kcal·mol^{-1} racemization will occur readily via the C_s symmetrical transition structure **8-TS1**. Structure **8a** is energetically favored by only 0.2 kcal·mol^{-1} over conformer **8b** in which the pyridine group has been transferred from an axial to an equatorial position. Racemization of this conformer has an even lower barrier of 9.6 kcal·mol^{-1}; **8-TS2** represents the C_s symmetrical transition structure for this process. Conformer **Δ8a** isomerizes into **Λ8b** and vice versa via the asymmetric transition structure **8-TS3**. This represents a turnstile rotation (TR), which is a single-step double Berry pseudorotation. Note that the mirror image of **8-TS3** reflects the enantiomeric rearrangement of **Λ8a** into **Δ8b**. The **8a**→**8b** barrier amounts to a modest 10.5 kcal·mol^{-1}, which concurs with the observed coalescence in the ^{1}H NMR spectrum. For the more sterically crowded **10**, which carries a phenyl substituent instead of a methyl, the isomerization barrier is even lower (9.5 kcal·mol^{-1}) due to the favorable electron-withdrawing properties of the axial phenyl ring.

An alternative path by which **8a** and **8b** can isomerize proceeds via a single-step Berry pseudorotation that has the square pyramidal **8-TS4** as transition structure (Figure 3, middle top). However, the barrier for this process is 4.3 kcal·mol^{-1} higher than it is for the turnstile rotation (**8-TS3**) because of friction between the aromatic *ortho*-hydrogens in the transition structure. For the more crowded **10** the corresponding difference in barrier heights of 5.7 kcal·mol^{-1} is even larger. These results concur with earlier findings that showed inversion pathways to be hampered by sterically more demanding ring systems[8] or with more electron withdrawing substituents.[11]

We wondered whether associative/dissociative lithium-nitrogen interactions might actually contribute to the dynamic behavior of the silicates. This doesn't appear to be the case as exchange of the Li^+ cation of **8** for the non-coordinating ammonium nBu$_4$N$^+$ cation did not show any change in the aromatic or methyl regions in the ^{1}H-NMR spectrum the resulting silicate **11**. Moreover, the ^{1}H-NMR spectrum of silicate **9** recorded at –70 °C (see SI) showed two signals that are assigned to the two CH_2 protons for the ethyl group. Apparently, at low temperatures the Berry pseudorotation and consequently racemization is hampered on the NMR time scale due to steric congestion, thereby causing different chemical environments for the two methylene protons.[8] Both these observations support the notion that the low-energy barriers for the Berry pseudorotations that interconnect the near-isoenergetic conformers are solely responsible for the broadening of the NMR resonances.

P-Containing Silicates 14 and 16 – Experimental

The next target is a silicate in which one of the two bidentate ligands contains a six-membered ring with a phosphorus atom. Instead of incorporating an aromatic phosphinine ring in analogy to the discussed pyridine approach, we opted for a different framework, one in which the phosphorus atom is embedded in the central ring of one of the bidentate ligands. In other words, the target silane precursor is **13** (Scheme 3). An added advantage of this choice is that it has the potential to provide insight into the influence of six vs. five membered ring coordination on the conformational dynamics of the silicate.

Spirosilane **13** was obtained in 87 % yield by reacting dichlorobiphenylsilane **4** with the Li_2-salt of bis(2-bromophenyl)-phenylphosphane **12**.[21] The molecular structure of **13**, obtained from a single-crystal X-ray structure determination, is

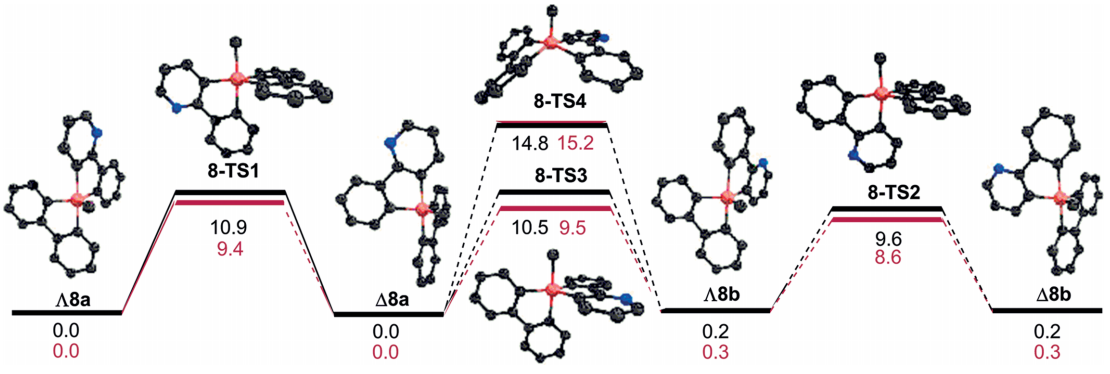

Figure 3. Isomerization of the conformers of **8** (black) and **10** (red) at B3LYP-D3/6-311++G(2p,d)//B3LYP/6-31G(d); energies in kcal·mol^{-1}. On the left are the enantiomeric pairs in which the pyridine group occupies an axial position and on the right where this group is located in an equatorial position.

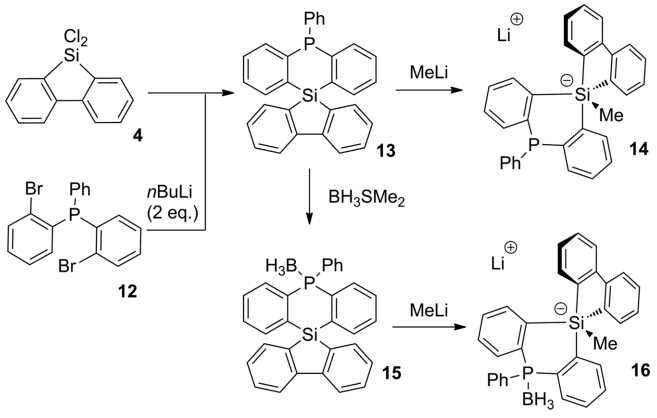

Scheme 3. Synthesis of silicates bearing a phosphorus atom in the scaffold.

shown on the left of Figure 4 and confirms the identity of the spirosilane. As expected, the six-membered heterocycle with its sp^3 hybridized phosphorus atom is slightly bent as reflected by the torsion angle between the two adjacent phenyl rings (∠ C81–P1–Si1–C21 151.27(4)°). The P-phenyl substituent is pointed in the opposite direction and "hoovers" over one side of the biphenyl group. All of this gives cause to complex ^{1}H and ^{13}C NMR spectra (see exp. section and SI).

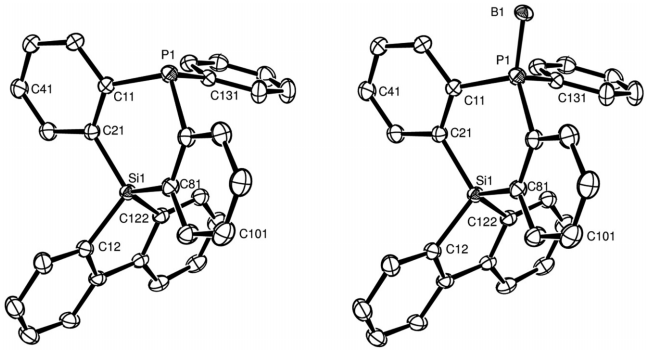

Figure 4. Molecular structures of **13** (left) and **15** (right) in their respective crystals (ellipsoids are set at 50 % probability; hydrogen atoms are omitted for clarity). Both compounds crystallize as racemates in centrosymmetric space groups. Selected bond lengths for **13** [Å] and angles [°]: Si1–C81 1.8661 (7), Si1–C12 1.8713 (8), P1–C131 1.8417 (8), P1–C11 1.8291 (7), C12–Si1–C122 91.26 (3), C12–Si1–C21 111.50 (3), C41–C21–C81 164.58, C21–Si1–C81 107.80 (3), C131–P1–C11 99.57 (3). Selected bond lengths for **15** [Å], angles and torsion angles [°]: Si1–C81 1.872 (9), Si1–C12 1.8641 (9), P1–B1 1.9149 (11), P1–C131 1.8150 (9), C12–Si1–C122 91.88 (4), C12–Si1–C21 111.24 (4), C41–C21–C81 162.23, C21–Si1–C81 106.57 (4), C131–P1–C11 103.84 (4), B1–P1–C131 111.02 (5), C41–C21–C81–C101 –2.3(3).

Formation of pentaorganosilicate **14** was pursued by reacting **13** with methyllithium but gave, however, a complex reaction mixture. Whereas no crystals suitable for an X-ray crystal structure analysis could be obtained from the extracted solid material, analysis of the NMR spectra proved to be revealing. The aliphatic region of the ^{1}H NMR spectrum showed two distinct signals at room temperature (Figure 5). Applying ^{1}H^{29}Si-HMBC revealed that the sharp ^{1}H NMR signal at 0.39 ppm corresponds to a ^{29}Si NMR chemical shift at 0.34 ppm, which is indicative for a tetracoordinated silicon (cf., δ = ^{29}Si **13** –19.9 ppm). This spectroscopy further revealed that the broad ^{1}H NMR singlet at 0.55 ppm showed only a Si-coupling at lower temperatures. For example, at –90 °C the broad ^{1}H NMR signal shifted downfield to a sharp singlet at 0.92 ppm that coupled with the ^{29}Si NMR chemical shift at –115.1 ppm, which we presume to be from silicate **14**. Cooling of the reaction mixture also showed a gradual decrease in intensity of the resonance at 0.39 ppm in favor of one at 0.24 ppm that is coupled with a ^{29}Si NMR chemical shift at –108.2 ppm, which could indicate the presence of an isomer of silicate **14**. Unfortunately, the reaction mixture proved to degrade rather quickly to an unknown ensemble of products, thereby inhibiting a more detailed analysis.

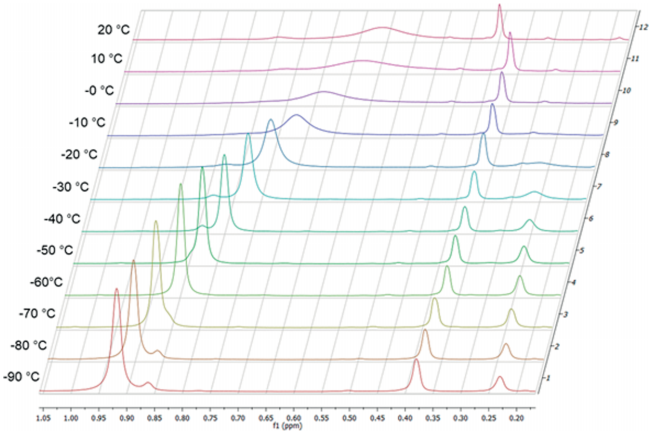

Figure 5. Aliphatic region of the ^{1}H-NMR spectrum of **14** measured at 10 °C intervals from 20 °C to –90 °C.

The variable temperature spectra shown in Figure 5 as well as the coupling of the ^{1}H NMR resonances with both tetra- and pentacoordinate silicon atoms suggest the presence of equilibria. To address the likely dynamic ^{1}H-NMR behavior of **14** we used a fitting program (NMRfit),[22] which revealed the sharp signals at 0.92 and 0.24 ppm (–70 °C) to originate from the broad signal at 0.55 ppm (20 °C). This isomerization process is well described by first order kinetics but only above –30 °C. An Eyring plot (see SI) suggests an activation barrier of 10.1 kcal·mol^{-1} for the isomerization and an energy difference of about 0.5 kcal·mol^{-1} between the two conformers. The low activation entropy of 1.6 cal·mol^{-1}·K^{-1} agrees with an unimolecular rearrangement. A second, higher order process gets involved at temperatures below –30 °C, causing the rate constants to deviate significantly from linearity. We interpret this behavior to be caused by ion-pairing as the chemical shifts of both signals move slightly upfield and the least-squares regression of this region in the Eyring plot shows a negative entropic contribution to the activation Gibbs free activation energy. It then seems that at decreasing temperatures (< –30 °C) ion exchange takes prevalence over conformational interchange.

To eliminate any possible interference of the phosphorus lone pair during the methylation of **13** with MeLi, we coordinated the P-center with a BH_3 group. Reaction of **13** with

BH_3·SMe_2 afforded the spirosilane precursor **15** in 91 % yield as a white crystalline solid. The molecular structure, obtained from a single-crystal X-ray structure determination, is shown on the right hand side of Figure 4. The differences with the BH_3 unprotected **13** are small. For example, the puckering angle of the phenyl flanked heterocycle is reduced from 151.27(4)° for **13** to 147.33(5)° for **15**, whereas its C-P–C bond angles are slightly larger (**13** 99.57(3)-104.97(3)°; **15** 103.84(4)-107.41(4)°). It is then not surprising that the ^1H and ^{13}C NMR spectroscopic differences between the two structures are only minimal.

Treatment of spirosilane **15** with MeLi provided silicate **16**, as a brown foam in ca. 90 % purity, presumably due to a reaction of MeLi with BH_3. Unfortunately, despite many attempts, no suitable crystals could be obtained for an X-ray crystal structure analysis. Nevertheless, NMR spectroscopic and DFT analyses provided much insight. The $^1H^{29}Si$-HMBC spectrum, shown in Figure 6, reveals the presence of two distinct silicates in a 1:1.7 ratio with characteristic signatures (δ = ^1H –0.64, δ = ^{29}Si –107.5 ppm; δ = ^1H 0.65, δ = ^{29}Si –110.6 ppm). We presume these silicates to be two conformers of **16** since they have the same exact mass. To assign these isomers, we discuss the results of the DFT analysis first (Figure 7).

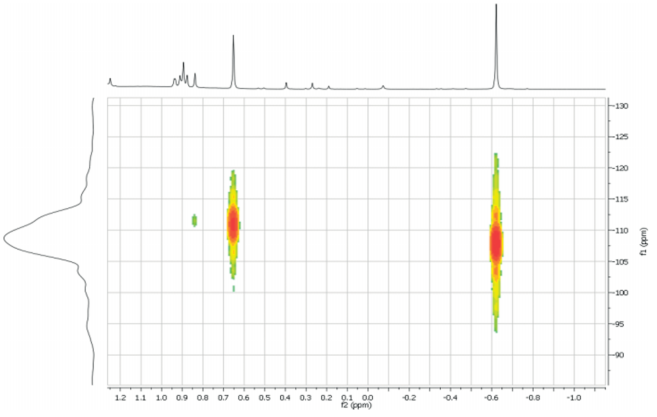

Figure 6. $^1H^{29}Si$-HMBC spectrum of BH_3-protected silicate **16**.

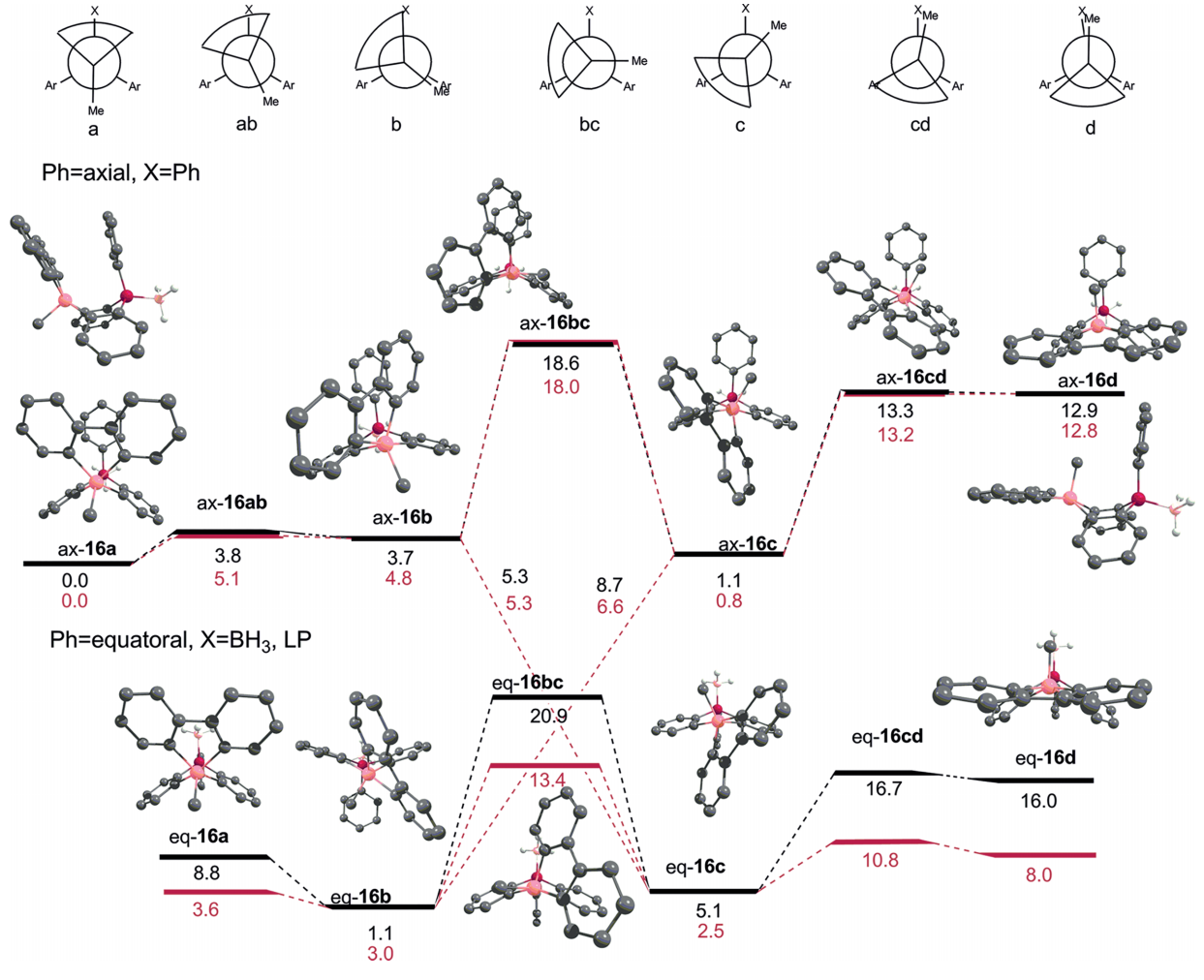

Figure 7. B3LYP-D3/6-311++G(2p,d)//B3LYP/6-31G(d) isomerizations of **14** (red) and **16** (black) with Berry pseudorotation transition structures. All energies (kcal·mol^{-1}) are relative to the lowest energy form. Silicon is colored light pink and phosphorus maroon. The P-Ph group is in an "axial" position in the upper part and in an "equatorial" position in the lower part (see text). X refers to the phosphorus BH_3 substituent (**16**) or its lone pair (**14**). The hatched lines that cross in the center represent the barriers for the interconversion of ax-**16(14)b** and eq –**16(14)c** and of ax-**16(14)c** and eq –**16(14)b**.

P-Containing Silicates 14 and 16 – Computational

Single point calculations were conducted for the silicates at B3LYP-D3/6-311++G(2p,d) on structures optimized at B3LYP/6-31G(d). The energy profiles for **14** (red) and the BH_3-stabilized **16** (black) are depicted in Figure 7. The very top of Figure 7 shows Newman projections along the imaginary Si–P axis. Their identifiers **a**, **b**, **c**, and **d** are associated with minima and those labeled **ab**, **bc**, and **cd** represent transition structures for Berry pseudorotations. Shown is the counterclockwise pseudorotation of the methyl and biphenyl substituents on silicon with respect to the dibenzo[*b*,*e*][1,4]phosphasilane unit; this motion represents an enantiomeric rotation of the chiral silicates with the clockwise motion representing the other. The upper energy diagram of Figure 7 shows the profile for structures with the P-Ph group oriented "orthogonally" to the carbon frame of the dibenzo[*b*,*e*]-[1,4]phosphasilane unit, whereas this orientation is "in-plane" for the bottom diagram; for simplicity they are labeled "Ph=axial" and "Ph=equatorial", respectively.

Energy Profile with Axial P-Ph

The lowest energy silicate structures ax-**14a** and ax-**16a** have C_s symmetry and a boat conformation for the dibenzo[*b*,*e*]-[1,4]phosphasilane unit. The "side view" of ax-**16a** in the top left of Figure 7 not only visualizes this boat form but also shows the stabilizing aromatic π-stacking of the P-phenyl substituent with the biphenyl ligand on Si. A square pyramidal conformation for a silicate's global energy minimum is unusual since it is typically associated with the transition structure for a Berry pseudorotation, but we presume the favored boat form of the dibenzo[*b*,*e*][1,4]phosphasilane unit in combination with advantageous dispersion forces to be responsible for this geometrical behavior.

The counterclockwise rotation of the Si-groups represents a Berry pseudorotation and gives the 3.7 (4.8) kcal·mol^{-1} less stable trigonal bipyramidal ax-**16b** (ax-**14b**) via a modestly higher barrier of only 3.8 (5.1) kcal·mol^{-1} (ax-**16ab** (ax-**14ab**)) as visualized by the Newman projections and the upper energy diagram in Figure 7. This Berry pseudorotation involves a change from a square pyramidal to a trigonal bipyramidal conformation that requires, of course, a change in C-Si-C angles around the silicon. This change is reflected in the increase of the angle between the methyl carbon, silicon, and one of the *ipso* carbon atoms of the biphenyl ligand that changes from 100.3° in ax-**16a** via 123.1° for ax-**16ab** to 134.4° in ax-**16b**.

Continuing the counterclockwise rotation results next in the 2.6 (4.0) kcal mol^{-1} more favorable ax-**16c** (ax-**14c**) that has a trigonal bipyramidal conformation around silicon with the two bidentate ligands in apical/equatorial positions. Whereas this conformer is just 1.1 (0.8) kcal·mol^{-1} less stable than the global minima, the Berry pseudorotation by which it is formed is the rate-determining step for isomerization of the silicate, requiring a significant 14.9 (13.2) kcal·mol^{-1}. One phenyl ring of the biphenyl ligand occupies the axial position of the distorted square pyramidal transition structure ax-**16bc** in which the equatorial methyl group is aligned almost parallel to the six membered P-containing ring. The sizeable pseudorotation barrier is caused by friction between the biphenyl ligand and the "axial" P-phenyl substituent.

Further continuing the rotation of the Si groups converts ax-**16c** (ax-**14c**) into the 11.8 (12.0) kcal·mol^{-1} less favorable ax-**16d** (ax-**14d**), which is unstable as the reverse motion requires a mere 0.4 kcal·mol^{-1} (ax-**16cd** and ax-**14cd**). The axial methyl group is aligned parallel to the P-Ph group in the square pyramidal structure, which contrasts the global minimum ax-**16a** that is stabilized by aromatic π-stacking (see the "side views" on the right and left of Figure 7). The pseudorotation causes a decrease of the C-Si–C angle between the methyl carbon and one of the ipso carbon atoms of the biphenyl ligand from 124.0° in ax-**16c** via 108.3° for ax-**16cd** to 96.6° in ax-**16d**, which is the opposite from that seen for ax-**16a** → [ax-**16ab**]‡ → ax-**16b**.

The described conversion of ax-**16a** (ax-**14a**) to ax-**16d** (ax-**14d**) reflects a 180° rotation in the Newman projections and shows little influence of whether or not the phosphorus atom carries the stabilizing BH_3 phenyl group. The rotation cycle is completed by mirroring the energy diagram to return to the global minimum. What still must be addressed is the P-Ph transfer into an "equatorial" position and its influence on the energy profile (bottom of Figure 7). This profile is distinctly different from that in which the P-Ph group is axially oriented.

Energy Profile with Equatorial P-Ph

In sharp contrast to the discussed ax-P-Ph energy profile, square pyramidal eq-**16a** (eq-**14a**) is a transition structure for the Berry pseudorotation that converts eq-**16b** (eq-**14b**) into its mirror image (ΔE 7.7 (0.6) kcal·mol^{-1} (Figure 7, bottom). We assume this difference in behavior to reflect the absence of stabilizing aromatic π-stacking. The rest of the energy profile shows resemblance to that for the conformers with ax-P-Ph orientations. Thus, the Berry pseudorotation of eq-**16b** into eq-**16c** is also associated with a sizeable barrier of 19.8 kcal·mol^{-1} and the subsequent clockwise rotation gives the energetically less favored square pyramidal eq-**16d**, just as is the case for the ax-P-Ph analogues. However, Berry pseudorotation of eq-**14b** into eq-**14c** has a distinctive lower barrier of 10.4 kcal·mol^{-1} (eq-**14bc)** probably due to less repulsion between the phosphorus lone pair and the substituents on Si. The most stable isomers on the eq-P-Ph energy profile are eq-**16b** and eq-**14c**, which are, respectively, only 1.1 and 2.5 kcal·mol^{-1} less stable than their global minima. The energy profiles for eq-**14** and eq-**16** differ mostly with respect to the Berry pseudorotation barriers which are significantly higher for the P-BH_3 stabilized silicate **16** due to steric repulsion.

Remains the question how the ax-P-Ph and eq-P-Ph energy profiles are connected. It is unlikely that this occurs through the square pyramidal conformers **a** and **d** as it would cause friction between the ortho hydrogens of the biphenyl ligand and the dibenzo[*b*,*e*][1,4]phosphasilane unit, but maybe more importantly eq-**16a** (eq-**14a**) is a transition structure and ax-**16d** (ax-**14d**) is a metastable conformer. The two energy profiles are instead connected through the trigonal bipyramidal conformers **b** and **c**. All what is needed is bending up the aromatic "wings" of the P-containing six-membered ring of ax-**16b**

(ax-**14b**) to give after reorientation eq-**16c** (eq-**14c**), which requires only a modest 5.3 (5.3) kcal·mol^{-1}. A similar ring flip converts eq-**16b** (eq-**14b**) into ax-**16c** (ax-**14c**) and has a comparable reaction barrier of 8.7 (6.6) kcal·mol^{-1}.

NMR-DFT Correlation

The presented DFT analysis of **14** is in excellent agreement with the energetic data that could be deduced from the limited VT ^{1}H NMR experiments that suggest, based on Eyring plots, an energy difference of ca. 0.5 kcal·mol^{-1} between two conformers and a barrier of ca. 10 kcal·mol^{-1} for their interconversion. Whereas the DFT potential energy surface for **14** might be complex, it identifies ax-**14a** and ax-**14c** as its two most stable conformers with a similarly small energy difference of only 0.8 kcal·mol^{-1}. The DFT calculations also give a similarly sized barrier of 13.4 kcal·mol^{-1} for the interchange of the conformers and illustrate the process to occur through a series of Berry pseudorotations and ring inversions, i.e., via ax-**14b**, eq-**14c**, and eq-**14b**.

The DFT calculations further enable the assignment of the two conformers of **16** observed at room temperature NMR as ax-**16a** and ax-**16c**; their computed energy difference amounts to 1.1 kcal·mol^{-1} with an interconversion barrier of 18.6 kcal·mol^{-1} (ax-**16bc**). Also the calculated ^{1}H NMR chemical shifts of ax-**16a** (0.76 ppm) and ax-**16c** (–0.71 ppm) agree well with the observed ones for the methyl group in **16** (0.65 ppm and –0.64 ppm). The phenyl ring in ax-**16c** hovers over the methyl group to cause significant shielding resulting in an upfield chemical shift at –0.64 ppm. This is not the case for the ax-**16a** isomer which has its Me resonance at a more common 0.65 ppm.

Conclusion

This study reports the first nonsymmetric single N and P atom containing organosilicates. One has a C,C-bridging 2-phenylpyridine group and the other a C,C-bridging triphenylphosphane with as remaining ligands a bidentate biphenyl and a methyl, ethyl, or phenyl group (**8–10**) or only a phenyl group (**14**). The stability of **14** increases by BH_3-substitution of its P-center (**16**). All pyridine containing silicates are remarkably stable with melting points ranging from 47 to 107° C for **8–10**. No melting point could be determined for foams **14**, and **16**. X-ray crystal structures are presented for **10, 13** and **15**.

Silicates **8–10** show dynamic conformational behavior in solution like the all-carbon silicate **2a**. They behave also similar to both the N- and S-hetero homologues **2b** and **2d** that have two hetero-containing C,C-bidentate ligands with five-membered pyrrole and thiophene rings, respectively. Replacing one phenyl group in **2a** for a pyridine group appears not to hamper the conformational dynamics of the system. VT NMR spectroscopic analysis revealed a rapid interchange of two isoenergetic conformers. DFT calculations estimate an energy difference of less than 0.5 kcal·mol^{-1} and an interconversion barrier of ca. 10 kcal·mol^{-1}, which is of the same magnitude as the racemization barriers for both conformers.

The P-containing silicates **14** and **16** behave differently because the phosphorus atom is embedded in the central six-membered ring of the C,C-chelating triphenylphosphane. VT NMR analysis revealed rapidly interchanging conformers for **14**, but also an equilibrium with its silane precursor. An Eyring plot suggests an energy difference of about 0.5 kcal·mol^{-1} between the two conformers and an interconversion barrier of ca. 10 kcal·mol^{-1}. DFT calculations confirm the presence of two isoenergetic conformers (ΔE < 1.0 kcal·mol^{-1}) and indicate a barrier of 13.4 kcal·mol^{-1} for a complex interconversion pathway that includes Berry pseudorotations, turnstile rotations, and "ring flips" of the dichelating six-membered Si,P-ring. Stabilizing the silicate by BH_3-coordination of the P-center (**16**) raises the lowest energy barrier for the complex interconversion to 18.6 kcal·mol^{-1}. This barrier is of the same general magnitude as reported for **2c**, which can be obtained as non-racemizing enantiomers if the fifth ligand is an equatorial fluorine. This bodes well for pursuing silicates with chiral integrity through either enlarging the size of the C,C-coordinating ring (**16**) or increasing the size of the ligand (**2c**).

We feel that the concepts outlined in this study on dynamic conformational behavior of nonsymmetric silicates may also be applicable to pentacoordinate transition metals and that it may contribute to enlarging the number chiral-at-metal catalysts.

Computational Section

Single-point density functional theory calculations were performed at the B3LYP[23–25]-D3[26]/6-311++G(2p,d) //B3LYP[27–29]/6-31G(d) level using the Gaussian09 suite of programs, revision D.01.[30] All geometry optimizations were carried out without symmetry restrictions and were performed at B3LYP/6-31G(d). The signature of all stationary points, minima and transition structures, were determined by through analytical calculation of the Hessian. at the same level of theory. Cartesian coordinates and total energies are provided for all structures in the Supporting Information. NMR chemical shifts have been calculated using the GIAO Method at the B3LYP/6-311++G(2p,d) level.[31-34]

Experimental Section

General. Tetrahydrofuran (THF) was distilled subsequently from $LiAlH_4$ and sodium/potassium alloy and diethyl ether from sodium/potassium alloy. *n*-Butyllithium and methyllithium were purchased as 1.6 M solutions in hexanes and in diethyl ether, respectively; ethyllithium was purchased as a 0.5 M solution in benzene/cyclohexane (9:1) Phenyllithium was purchased as a 1.9 M solution in di-*tert*-butyl ether. Tetrachlorosilane was distilled and refluxed before use to remove HCl. The mass, NMR and melting point samples of silicates were prepared and handled in the purified N_2 atmosphere of an MBRAUN Unilab glovebox; other syntheses were performed using standard Schlenk techniques. NMR spectra were recorded on a Bruker Avance 400 (^{1}H, ^{13}C, ^{31}P{^{1}H}, ^{11}B{^{1}H},^{29}Si,2D spectra) or Bruker Avance 500 (^{1}H, ^{13}C). NMR chemical shifts are internally referenced to the solvent for ^{1}H ($CHCl_3$: 7.26, THF: 3.59, CH_2Cl_2: 5.32 ppm) and ^{13}C ($CHCl_3$: 77.16, THF: 67.58, CH_2Cl_2: 53.84 ppm), and externally for ^{29}Si, ^{31}P{^{1}H}, ^{11}B{^{1}H} to TMS, 85 % H_3PO_4 and

BF_3·OEt_2, respectively. Melting points were measured on samples in sealed capillaries and are uncorrected. HR-ESI-MS measurements of silicates were measured on an AccuTof JMS-T 100LP mass spectrometer.

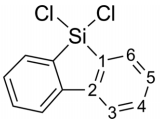

5,5-Dichloro-5H-dibenzo[b,d]silole (**5**). 2,2-dibromobiphenyl (6.14 g, 19.69 mmol, 1.0 eq.) was dissolved in THF (55 mL) and cooled to –78 °C. To this colorless solution, *n*BuLi (25.48 mL, 40.76 mmol, 2.07 eq.) was added and the mixture was stirred for one hour at –78 °C. Silicontetrachloride (11.28 mL, 98.47 mmol, 5.0 eq.) was separately dissolved in THF (30 mL) and cooled to –95 °C. The yellow suspension of the 2,2-dilithumbiphenyl was added dropwise to this colorless solution and the mixture was stirred overnight, gradually warming to room temperature. Next, all volatiles were removed in vacuo and the product was extracted into Et_2O (3 × 20 mL). The product was obtained as a impure white solid after evaporation of residual solvent in vacuo. Yield: 4.44 g (17.0 mmol, 86 %). ^{1}H NMR (500.23 MHz, [D_8]THF): δ = 7.92 (d, ^3J(H,H) = 7.8 Hz, 2H; H3), 7.75 (d, ^3J(H,H) = 7.1 Hz, 2H; H6), 7.56 (dt, ^3J(H,H) = 7.7 Hz, ^4J(H,H) = 1.2 Hz, 2H; H4), 7.39 (dt, ^3J(H,H) = 7.4 Hz, ^4J(H,H) = 0.9 Hz, 2H; H5). ^{13}C{^{1}H} NMR (125.78 MHz, [D_8]THF, 296 K): δ = 146.38 (C2), 134.04 (C4), 133.11 (C6), 130.98 (C1), 129.76 (C5), 122.09 (C3). ^{1}H-^{29}Si-HMBC NMR (400.13, 79.49 MHz, [D_8]THF, 295 K): δ = 6.16. Mp: 92.1–101.6 °C.

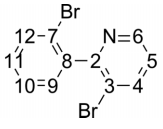

3-Bromo-2-(2-bromophenyl)pyridine **6**: prepared according to a literature procedure.[35] 2,3-Dibromopyridine **7** (1.00 g, 4.22 mmol) and 2-bromo-phenylboronic acid (854 mg, 4.22 mmol) were dissolved in tetrahydrofuran (20 mL), aqueous K_2CO_3 (1 M, 15 mL), 5 drops of aqueous KOH (10 %) and then degassed. $Pd(PPh_3)_4$ (244 mg, 0.21 mmol) was added and the yellow mixture was refluxed for 72 h. After cooling, the phases were separated and the aqueous phase was extracted three times with chloroform. The combined organic phases were dried with Na_2SO_4 and concentrated under vacuum. The crude mixture was separated by column chromatography (SiO_2, cHex/EtOAc, 2:1, Rf = 0.38), giving 1.22 g (92 %) of product **6** as a colorless oil, which solidified overnight. ^{1}H NMR (500.23 MHz, CD_2Cl_2, 296 K): δ 8.62 (dd, ^3J(H,H) = 5.0 Hz, ^4J(H,H) = 1.0 Hz, 1H; H6), 8.01 (dd, ^3J(H,H) = 8.0 Hz, ^4J(H,H) = 1.0 Hz, 1H; H4), 7.68 (dd, ^3J(H,H) = 8.5 Hz, ^4J(H,H) = 1.0 Hz, 1H; H12), 7.46–7.43 (m, 1H; H10), 7.35–7.31 (m, 2H; H9, H11), 7.25 (dd, ^3J(H,H) = 8.0 Hz, ^4J(H,H) = 5.0 Hz, 1H; H5); ^{13}C{1H} NMR (125.78 MHz, CD_2Cl_2, 296 K): δ 158.65 (C2), 148.23 (C6), 141.52 (C8), 140.66 (C4), 132.89 (C12), 130.63 (C9 or C11), 130.39 (C9 or C11), 127.71 (C10), 124.60 (C5), 122.63 (C7), 121.49 (C3); HR-MS (ESI): calcd. for $C_{11}H_9Br_2N$ 311.9018, found 311.9017.

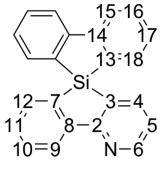

2-Pyridylphenyl-biphenyl-2,2′-silane **7**: *n*BuLi (8.24 mL, 13.23 mmol, 2.07 eq.) was added to a solution of **6** (2.0 g, 6.39 mmol, 1.0 eq.) in Et_2O (80 mL) and cooled to –78 °C, the yellow suspension was stirred at –78 °C for 90 min. In a separate Schlenk vessel, **5** (1.6 g, 6.39 mmol, 1.0 eq.) was dissolved in Et_2O (60 mL), cooled to 0 °C and the lithiated suspension of **6** was added dropwise to the colorless solution of **5** at 0 °C. The resulting orange/red suspension was stirred overnight at room temperature, quenched using water, extracted into Et_2O (× 3), dried with Na_2SO_4, filtered and concentrated in vacuo. The orange residue was purified using column chromatography (cHex/EtOAc, first 10/0, then 10/1, 9/1, 8/1), concentrated in vacuo and washed using *n*-pentane to obtain product **7** as a white solid. (558.5 mg, 1.67 mmol, 52 %). ^{1}H NMR (500.23 MHz, CD_2Cl_2, 296 K): δ 8.56–8.65 (m; H6), 8.33 (d, ^3J(H,H) = 8.0 Hz, 1H; H9), 7.96 (d, ^3J(H,H) = 7.5 Hz, 2H; H15), 7.68 (dd, ^3J(H,H) = 7.0 Hz, ^4J(H,H) = 1.5 Hz, 1H; H4), 7.58 (t, ^3J(H,H) = 7.5 Hz, 1H; H10), 7.53 (t, ^3J(H,H) = 7.5 Hz, 2H; H16), 7.42–7.38 (m, 3H; H12, H18), 7.33 (t, ^3J(H,H) = 7.5 Hz, 1H; H11), 7.23 (t, ^3J(H,H) = 7.5 Hz, 2H; H17), 7.12–7.10 (m, 1H; H5). ^{13}C{^{1}H} NMR (125.78 MHz, CD_2Cl_2, 296 K): δ 167.54 (C2), 152.10 (C6), 150.55 (C8), 150.44 (C14), 142.20 (C4), 134.50 (C18), 134.23 (C12), 133.39 (C7), 132.09 (C10), 132.01 (C16), 131.92 (C13), 129.97 (C11), 128.43 (C17), 127.21 (C3), 122.98 (C5, C9), 121.59 (C15); ^{1}H-^{29}Si-HMBC NMR (400.13, 79.49 MHz, CD_2Cl_2, 296 K): δ –9.21 (Si); IR (neat): $\tilde{\nu}$ = 3040 (w, C-H_{Ar}), 820 (m, C_{Ar}-H), 758 (s, C_{Ar}-H); $C_{23}H_{16}NSi$ 334.1047, found 334.1043. Mp 216.1 °C.

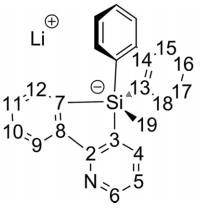

Lithium methyl-2-pyridylphenyl-biphenyl-2,2′-silicate **8**: MeLi (1.6 M in Et_2O, 0.098 mL, 0.16 mmol, 1.05 eq.) was added to a solution 2-pyridylphenyl-biphenyl-2,2′-silane **6** (50mg, 0.15 mmol, 1.0 eq.) in THF (1 mL) at –78 °C. The resulting yellow solution was stirred for 0.5 hour at this temperature and warmed to r.t. The orange solution was concentrated in vacuo and the resulting orange foam was washed with *n*-pentane to obtain **8** as a bright yellow powder (98.3 mg, quant. with excess MeLi). ^{1}H NMR (500.23 MHz, [D_8]THF, 269 K) δ = 8.19 (dd, ^3J(H,H) = 4.7 Hz, ^4J(H,H) = 1.7 Hz, 1H), 8.14 (d, ^3J(H,H) = 7.6 Hz, 1H), 7.77 (br. s, 1H), 7.70 (d, ^3J(H,H) = 7.7 Hz, 2H; H18), 7.56 (d, ^3J(H,H) = 7.0 Hz, 1H), 7.52 (d, ^3J(H,H) = 6.3 Hz, 2H), 7.07–7.02 (m, 2H; H17), 6.90 (br. s, 4H), 0.35 (s, 3H; H19). ^{13}C{^{1}H} NMR (125.78 MHz, [D_8]THF, 296 K): δ 136.32 (CH), 124.96 (C18), 120.83 (bs), 119.40 (C17), 7.03 (C19), the signals for C1 to C 16 were unresolved. ^{1}H-^{29}Si-HMBC NMR (400.13, 79.49 MHz, [D_8]THF, 296 K): δ –107.2 (Si). HR-MS (ESI): calcd. for $C_{24}H_{18}NSi$ 348.1214, found 348.1214. Mp: >47.2 °C (decomp.).

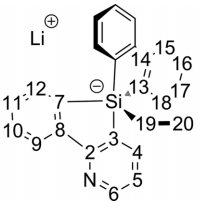

Lithium methyl-2-pyridylphenyl-biphenyl-2,2′-silicate **9**: EtLi (0.5 M, 0.36 mL, 1.2 eq.) was added to a solution of 2-pyridylphenyl-biphenyl-2,2′-silane **6** (50 mg, 0.15 mmol, 1.0 eq.) in THF (1 mL) at –78 °C. The resulting yellow solution was stirred for 0.5 hour at this temperature and warmed to r.t The orange solution was concentrated in vacuo and the orange foam was washed using *n*-pentane

to obtain **9** as a slightly yellow powder (84.3 mg, 0.13 mmol, 85.4 %). ^{1}H NMR (400.13 MHz, [D$_8$]THF, 269 K): δ = 8.20 (dd, ^3J(H,H) = 4.6 Hz, ^4J(H,H) = 0.8 Hz, 1H), 8.16 (d, ^3J(H,H) = 7.2 Hz, 1H), 7.87–7.82 (m, 1H), 7.70 (d, ^3J(H,H) = 7.8 Hz, 2H; H18), 7.64 (d, ^3J(H,H) = 7.0 Hz, 1H), 7.60 (d, ^3J(H,H) = 6.0 Hz, 2H), 7.09–7.01 (m, 2H; H17), 6.90 (br. s, 4H), 0.93–0.88 (m, 2H; H19), 0.73 (t, ^3J(H,H) = 7.5 Hz, 3H; H20). ^{13}C NMR (100.6 MHz, [D$_8$]THF, 269 K): δ 122.08 (CH), 118.43 (CH), 116.54 (CH), 13.84 (C19), 8.06 (C20), the signals for carbon 1 to 18 were unresolved. ^{1}H-^{29}Si-HMBC NMR (400.13, 79.49 MHz, [D$_8$]THF, 296 K): δ –101.6 (Si). HR-MS (ESI): calcd. for $C_{25}H_{20}NSi$ 362.1370, found 362.1386. Mp: >77.6 °C (decomp.).

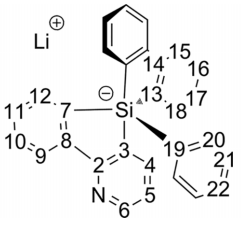

Lithium phenyl-2-pyridylphenyl-biphenyl-2,2′-silicate **10**: PhLi (1.9 M, 0.082 mL, 0.16 mmol, 1.05 eq.) was added to a solution 2-pyridyl-phenyl-biphenyl-2,2′-silane **6** (50 mg, 0.15 mmol, 1.0 eq.) in THF (1 mL) at –78 °C. The resulting dark red solution was stirred for 0.5 hour at this temperature and warmed to r.t. The mixture was then warmed to r.t. and became a dark brown solution, which gave a brown foam-like solid after concentration in vacuo. The product was obtained with some excess PhLi present. ^{1}H NMR (400.13 MHz, [D$_8$]THF) δ = 8.21 (d, ^3J(H,H) = 7.5 Hz, 1H), 8.18 (dd, ^3J(H,H) = 4.8 Hz, ^4J(H,H) = 1.8 Hz, 1H), 7.74 (d, ^3J(H,H) = 7.6 Hz, 2H), 7.47 (d, ^3J(H,H) = 6.0 Hz, 1H), 7.43–7.42 (m, 1H), 7.30 (d, ^3J(H,H) = 6.0 Hz, 2H), 7.10 (t, ^3J(H,H) = 7.0 Hz, 1H). 7.06–7.02 (m, 4H), 6.90 (dt, ^3J(H,H) = 7.1 Hz, ^4J(H,H) = 0.9 Hz, 1H), 6.82 (t, ^3J(H,H) = 7.0 Hz, 1H), 6.73–6.70 (m, 3H). ^{1}H-^{29}Si-HMBC NMR (400.13, 79.49 MHz, [D$_8$]THF, 296 K): δ –102.2 (Si). HR-MS (ESI): calcd. for $C_{29}H_{20}NSi$ 410.1370, found 410.1373. Mp: >107.3 °C (decomp.).

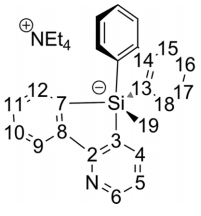

Tetraethylammonium methyl 2-pyridylphenyl-biphenyl-2,2′-silicate **11**: MeLi (1.6 M in Et$_2$O, 0.098 mL, 1.05 eq.) was added to a solution 2-pyridylphenyl-biphenyl-2,2′-silane **6** (50 mg, 0.15 mmol, 1.0 eq.) in THF (1 mL) at –78 °C. The resulting yellow solution was stirred for 0.5 hour at this temperature and warmed to r.t. Tetraethylammonium bromide was suspended separately in THF (2 mL) and the yellow silicate solution was added to this mixture. The suspension turned darker yellow and was stirred overnight at r.t. Volatiles were evaporated in vacuo and the white foam was washed with Et$_2$O to yield **11** as a white solid with 15 % hydrolysis (quant.). ^{1}H NMR (400.13 MHz, [D$_8$]THF, 269 K) δ = 8.22 (dd, ^3J(H,H) = 4.4 Hz, ^4J(H,H) = 1.6 Hz, 1H), 8.14 (d, ^3J(H,H) = 7.6 Hz, 1H), 7.74–7.71 (m, 2H, H18), 7.51–7.46 (m, ^3J(H,H) = 7.0 Hz, 3H), 7.11–7.04 (m, 2H, H17), 6.90 (br. s, 4H), 3.32 (q, ^2J(H,H) = 14.5 Hz, ^3J(H,H) = 7.4 Hz, 8H), 1.23–1.19 (m, 12H), 0.31 (s, 3H; H19).

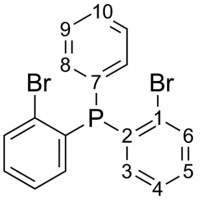

Bis(2-bromophenyl)(phenyl)phosphane (**12**):[36] 1,2-dibromobenzene (2.8 mL, 23.30 mmol, 2.03 eq.) was dissolved in THF (40 mL) and Et$_2$O (40 mL) and cooled to –115 °C. To this colourless solution *n*BuLi (14.56 mL, 23.30 mmol, 2.03 eq.) was added dropwise at a rate of 0.15 mL/min after which the resulting white suspension was stirred for one hour. Dichlorophenylphosphane (1.55 mL, 11.50 mmol, 1.0 eq.) was added dropwise to the suspension and stirred for 30 minutes. The orange solution was stirred overnight, gradually increasing the temperature to room temperature. Afterwards, aqueous NH_4Cl was added and the product was extracted into DCM, the organic layer was dried with Na_2SO_4 and filtered. After evaporation of the solvents, the white product was purified by washing with pentane and cold methanol. Yield: (2.79 g, 6.64 mmol, 58 %). ^{1}H NMR (500.23 MHz, $CDCl_3$): δ = 7.64–7.60 (m, 2H; H6), 7.44–7.37 (m, 3H; H8, H10), 7.29 (td, ^3J(H,H) = 8.1 Hz, ^4J(H,H) = 1.4 Hz, 2H; H9), 7.24–7.20 (m, 4H; H4, H5), 6.77–6.73 (m, 2H; H3). ^{13}C{^{1}H} NMR (125.78 MHz, $CDCl_3$): δ = 137.9 (d, ^1J(C,P) = 11.0 Hz; C2), 137.70 (C3), 134.54 (d, ^3J(C,P) = 21.5 Hz; C9), 133.23 (d, ^3J(C,P) = 2.5 Hz; C6), 130.56 (s; C5), 130.21 (d, ^2J(C,P) = 32.4 Hz; C1), 129.58 (C10), 129.03 (d, ^2J(C,P) = 7.7 Hz, C8), 127.71 (C4), the signal for C7 was unresolved. ^{31}P NMR (162.0 MHz, $CDCl_3$): δ = –4.17. Mp: 123.7 °C (decomp).

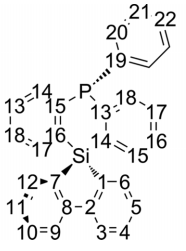

5′-Phenyl-5′H-spiro[dibenzo[b,d]silole-5,10′-dibenzo-[b,e][1,4]phosphasilane] (**13**): *n*BuLi (11.97 mL, 19.15 mmol, 2.07 eq.) was added dropwise to a solution of bis(2-bromophenyl)phenylphosphane (3.88 g, 9.25 mmol, 1.0 eq.) in THF (140 mL) at –78 °C and the orange solution was stirred for one hour. Separately, 5,5-dichlorodibenzosilole (2.42 g, 9.25 mmol, 1.0 eq.) was dissolved in THF (70 mL) and cooled to –78 °C, after which the yellow solution was added to the orange solution. The resulting dark red solution was stirred overnight, gradually letting the mixture reach room temperature. Afterwards, the product was filtered through a plug of alumina and solvents were removed in vacuo. The product was purified by dissolving it in little amount of DCM, followed by precipitation in *n*-pentane. The product was obtained as a pure white solid (3.56 g, 8.08 mmol, 87 %). ^{1}H NMR (500.23 MHz, $CDCl_3$): δ = 7.95 (dd, ^3J(H,H) = 7.8, ^4J(H,H) = 2.8 Hz, 2H; H3, H9), 7.61 (d, ^3J(H,H) = 7.1 Hz, 1H; H12), 7.52 (t, ^3J(H,H) = 9.0 Hz, 2H; H18), 7.42 (m, 2H; H4, H10), 7.35 (m, 9H; H17, H15, H20, H21, H22), 7.18 (m, 3H; H11, H16), 7.05 (t, ^3J(H,H) = 6.9 Hz, 1H; H5), 6.62 (d, ^3J(H,H) = 7.1 Hz, 1H; H6). ^{13}C{^{1}H} NMR (125.78 MHz, $CDCl_3$): δ = 149.86 (C2), 149.16 (C8), 146.75 (d, ^1J(C,P) = 11.6 Hz; C13),140.75 (d, ^1J(C,P) = 15.0 Hz; C19), 136.51 (C7), 135.26 (d, ^2J(C,P) = 3.1 Hz; C20), 134.47–134.40 (m; C1, C14), 134.37 (C6), 134.07 (C12), 134.01 (d, ^3J(C,P) = 3.8 Hz; C15), 133.48 (d, ^2J(C,P) = 3.8 Hz; C18), 130.91 (C4 or C10) 130.85 (C4 or C10), 129.45

(d; ^3J(C,P) = 10.0 Hz; C17), 128.85–128.76 (m; C21, C22), 127.85 (C16), 127.56 (C5, C11), 121.02 (C3 or C9), 120.89 (C3 or C9).* ^{1}H-^{29}Si-HMBC NMR (400.13, 79.49 MHz, $CDCl_3$, 295 K): δ = –19.40. ^{31}P NMR (162.0 MHz, THF d8): δ = –6.76. MP: 192.2–195.5 °C.

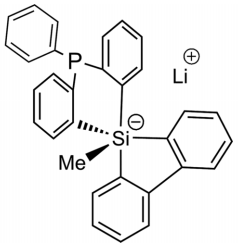

Triphenylphosphanemethylsilicate **14**: MeLi (1.6 M in Et_2O, 0.078 mL, 0.12 mmol, 1.1 eq.) was added dropwise to a solution of triphenylphosphanesilane **13** (50.0 mg, 0.11 mmol, 1.0 eq.) in THF (1 mL) at –78 °C. The pink solution was stirred for 30 minutes at this temperature and for 30 minutes at r.t. Volatiles were removed in vacuo and the remaining red solid was washed with pentane (3 × 5 mL), obtaining a complex mixture of **14** in various forms as a brown foam (quant). ^{1}H NMR (400.13 MHz, [D$_8$]THF, 183 K): complex aromatic region, 0.92 (H), 0.38 (H), 0.23 (H). ^{29}Si NMR (162.0 MHz, [D$_8$]THF, 183 K): δ = –115.1 (Si), –107.6 (Si), 0.9 (Si).

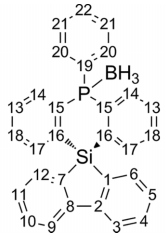

Borane triphenylphosphanesilane **15**: BH_3SMe_2 (2.86 mL, 5.72 mmol, 4.0 eq.) was added dropwise to a colorless solution of triphenylphosphanesilane **13** (0.63 g, 1.43 mmol, 1.0 eq.) in THF (60 mL) at 0 °C. The colorless solution was stirred overnight, gradually warming to room temperature. Afterwards, H_2O was added, the mixture was extracted into DCM and solvents were removed in vacuo. Product was purified by washing with pentane to obtain **15** as a pure white solid (0.59 g, 1.29 mmol, 91 %). ^{1}H NMR (500.23 MHz, [D$_8$]THF): δ = 8.31 (dd, ^2J(H,P) = 12.1 Hz, ^3J(H,H) = 7.7 Hz, 2H; H14), 7.99 (d, ^3J(H,H) = 7.8 Hz, 1H; H9), 7.91 (d, ^3J(H,H) = 8.1 Hz, 1H; H3), 7.62 (tt, ^3J(H,H) = 7.7 Hz, ^3J(H,P) = 1.4 Hz, 2H; H13), 7.55–7.49 (m, 3H; H10, H12, H22), 7.43–7.39 (m, 4H; H18, H21), 7.36–7.33 (m, 3H; H17, H4), 7.29–7.25 (m, 3H; H20, H11), 6.82 (t, ^3J(H,H) = 7.2 Hz, ^4J(H,H) = 0.6 Hz, 1H; H5), 5.82 (dd, ^3J(H,H) = 7.3 Hz, ^4J(H,H) = 0.5 Hz, 1H; H6), 1.37 (br.s, 3H; BH_3). ^{13}C{^{1}H} NMR (125.78 MHz, [D$_8$]THF): δ = 151.09 (C8), 150.42 (C2), 137.84 (d, ^1J(C,P) = 56.9 Hz; C19), 137.50 (d, ^2J(C,P) = 4.2 Hz; C16), 137.13 (d, ^3J(C,P) = 7.6 Hz; C17), 136.43 (d, ^1J(C,P) = 54.46 Hz; C19), 135.74 (C7), 135.72 (d, ^2J(C,P) = 15.4 Hz; C14), 135.48 (C22), 134.88 (C6), 133.38 (d, ^2J(C,P) = 9.5 Hz; C20), 132.55 (C12), 132.04 (C4), 131.56–131.41 (m; C10, C13, C18), 130.02 (d, ^2J(C,P) = 9.9 Hz; C21), 129.36 (C11), 128.57 (C5), 122.15 (C3), 122.04 (C9). ^{1}H-^{29}Si-HMBC NMR (400.13, 79.49 MHz, [D$_8$]THF): δ = –21.6. ^{31}P NMR (162.0 MHz, [D$_8$]THF): δ = 10.53. ^{11}B NMR (128.3 MHz, $CDCl_3$): δ = –36.54. HR-MS (EI): calcd. for $C_{30}H_{24}BPSi$ 454.1478 and $C_{30}H_{21}PSi$ 440.1150, found 454.1481 and 440.1116.

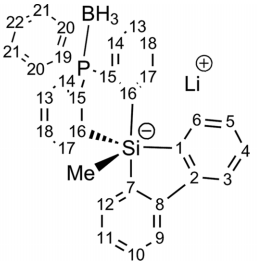

Borane triphenylphosphanemethylsilicate **16**: MeLi (0.078 mL, 0.12 mmol, 1.1 eq.) was added dropwise to a solution of borontriphenylphosphanesilane **15** (50.0 mg, 0.11 mmol, 1.0 eq.) in THF (1 mL) at –78 °C. The pink solution was stirred for 30 minutes at –78 °C and for 30 minutes at r.t. Volatiles were removed in vacuo and the red solid was washed with *n*-pentane (3 × 5 mL) to afford crude **16** as a syn/anti mixture in a 1:0.6 ratio; the ratio is based on integration of the respective ^{31}P NMR signals). The product was found to contain multiple impurities which could not be removed by washing steps or by crystallization. As a result, full characterization by means of ^{1}H and ^{13}C NMR spectroscopy was hampered; the recorded spectra are presented below and show multiple overlapping signals in the aromatic region. However, the two ^{1}H NMR resonance signals corresponding to the –CH_3 groups in **16-syn** and **16-anti** could be located at –0.64 ppm and 0.65 ppm, respectively. These values were found to be in good agreement with the values obtained from NMR calculations using DFT (GIAO method; δ = ^{1}H NMR calcd. –CH_3 **16-syn** = –0.71 ppm; **16-anti** = 0.76 ppm). The product was further identified by heteronuclear NMR spectroscopy in combination with HR-MS. ^{1}H-^{29}Si-HMBC NMR (400.13, 79.49 MHz, [D$_8$]THF): δ = –110.6, –107.5. ^{31}P NMR (162.0 MHz, [D$_8$]THF): δ = 2.75 (s) and 0.20 (s) in a 1:0.6 ratio. ^{11}B{^{1}H} NMR (128.3 MHz, [D$_8$]THF): δ = –37.16 (s). HR-MS (CSI): calcd. for $C_{31}H_{27}BPSi$ 469.1718 ([M]– –[CH_3]–), found 469.1734; calcd. for $C_{31}H_{24}PSi$ 455.1390 ([M] – –[CH3]– –BH_3), found 455.1415.

CCDC 1901693 (for **10**), 1901694 (for **13**), and 1901695 (for **15**) contain the supplementary crystallographic data for this paper. These data can be obtained free of charge from The Cambridge Crystallographic Data Centre.

Acknowledgments

This work was supported by The Netherlands Organisation for Scientific Research, Chemical Sciences (NWO-CW). We acknowledge SARA Computing and Networking Services for computer time.

Keywords: Silicon · Silicates · Hypervalent compounds · Berry pseudorotation · Density functional calculations

[1] J. Wagler, U. Böhme, E. Kroke, in *Funct. Mol. Silicon Compd. I* (Ed. D. Scheschkewitz), Springer International Publishing, **2013**, pp. 29–105.
[2] G. Singh, G. Kaur, J. Singh, *Inorg. Chem. Commun.* **2018**, *88*, 11–20.
[3] K. Lammertsma, E. P. A. Couzijn, J. C. Slootweg, A. W. Ehlers, *Z. Anorg. Allg. Chem.* **2009**, *635*, 1273–1278.
[4] E. P. A. Couzijn, A. W. Ehlers, M. Schakel, K. Lammertsma, *J. Am. Chem. Soc.* **2006**, *128*, 13634–13639.
[5] The stability of the silicates improves on exhanging the hard Li^+ counterion for the softer nBu_4N^+ ion.
[6] S. Deerenberg, M. Schakel, A. H. J. F. de Keijzer, M. Kranenburg, M. Lutz, A. L. Spek, K. Lammertsma, *Chem. Commun.* **2002**, 348–349.
[7] D. Ballweg, Y. Liu, I. A. Guzei, R. West, *Silicon Chem.* **2002**, *1*, 55–58.

[8] E. P. A. Couzijn, D. W. F. van den Engel, J. C. Slootweg, F. J. J. de Kanter, A. W. Ehlers, M. Schakel, K. Lammertsma, *J. Am. Chem. Soc.* **2009**, *131*, 3741–3751.
[9] E. P. A. Couzijn, M. Schakel, F. J. J. de Kanter, A. W. Ehlers, M. Lutz, A. L. Spek, K. Lammertsma, *Angew. Chem. Int. Ed.* **2004**, *43*, 3440–3442; *Angew. Chem.* **2004**, *116*, 3522.
[10] S. Ishida, M. Takiguchi, T. Iwamoto, *Heteroat. Chem.* **2018**, *29*, e21481.
[11] L. J. P. van der Boon, L. van Gelderen, T. R. de Groot, M. Lutz, J. C. Slootweg, A. W. Ehlers, K. Lammertsma, *Inorg. Chem.* **2018**, *57*, 12697–12708.
[12] S. Kojima, K. Kajiyama, M. Nakamoto, K. Akiba, *J. Am. Chem. Soc.* **1996**, *118*, 12866–12867.
[13] J. Ma, X. Zhang, X. Huang, S. Luo, E. Meggers, *Nat. Protoc.* **2018**, *13*, 605–632.
[14] M. Fontecave, O. Hamelin, S. Ménage, *Top. Organomet. Chem.* **2005**, *15*, 271–288.
[15] L. Gong, L.-A. Chen, E. Meggers, *Angew. Chem. Int. Ed.* **2014**, *53*, 10868–10874; *Angew. Chem.* **2014**, *126*, 11046.
[16] Z.-Y. Cao, W. D. G. Brittain, J. S. Fossey, F. Zhou, *Catal. Sci. Technol.* **2015**, *5*, 3441–3451.
[17] L. Zhang, E. Meggers, *Chem. Asian J.* **2017**, *12*, 2335–2342.
[18] S. Seesukphronrarak, T. Takata, *Chem. Lett.* **2007**, *36*, 1138–1139.
[19] S. J. Aspin, S. Taillemaud, P. Cyr, A. B. Charette, *Angew. Chem. Int. Ed.* **2016**, *55*, 13833–13837; *Angew. Chem.* **2016**, *128*, 14037.
[20] It is noteworthy that treatment of **5** with *n*BuLi and $SiCl_4$ did not give spirosilane **7** with two pyridine groups, but instead only a complex product mixture.
[21] Reaction of **4** with 2 equiv. of the Li_2-salt of **12** did not give the spirosilane with two equivalent bidentate P-containing ligands but instead a complex mixture of products.
[22] S. O. O'Kennedy, W. J. Gerber, *NMRfit*, The Mathlab Works, Inc. **1984**.
[23] A. D. Becke, *J. Chem. Phys.* **1993**, *98*, 5648–5652.
[24] S. H. Vosko, L. Wilk, M. Nusair, *Can. J. Phys.* **1980**, *58*, 1200–1211.
[25] C. Lee, W. Yang, R. G. Parr, *Phys. Rev. B* **1988**, *37*, 785–789.
[26] S. Grimme, J. Antony, S. Ehrlich, H. Krieg, *J. Chem. Phys.* **2010**, *132*, 154104.
[27] A. D. McLean, G. S. Chandler, *J. Chem. Phys.* **1980**, *72*, 5639–5648.
[28] R. Krishnan, J. S. Binkley, R. Seeger, J. A. Pople, *J. Chem. Phys.* **1980**, *72*, 650–654.
[29] P. J. Stephens, F. J. Devlin, C. F. Chabalowski, M. J. Frisch, *J. Phys. Chem.* **1994**, *98*, 11623–11627.
[30] M. J. Frisch, G. W. Trucks, H. B. Schlegel, G. E. Scuseria, M. A. Robb, J. R. Cheeseman, G. Scalmani, V. Barone, B. Mennucci, G. A. Petersson, H. Nakatsuji, M. Caricato, X. Li, H. P. Hratchian, A. F. Izmaylov, J. Bloino, G. Zheng, J. L. Sonnenberg, M. Hada, M. Ehara, K. Toyota, R. Fukuda, J. Hasegawa, M. Ishida, T. Nakajima, Y. Honda, O. Kitao, H. Nakai, T. Vreven, J. A. Montgomery Jr., J. E. Peralta, F. Ogliaro, M. Bearpark, J. J. Heyd, E. Brothers, K. N. Kudin, V. N. Staroverov, R. Kobayashi, J. Normand, K. Raghavachari, A. Rendell, J. C. Burant, S. S. Iyengar, J. Tomasi, M. Cossi, N. Rega, J. M. Millam, M. Klene, J. E. Knox, J. B. Cross, V. Bakken, C. Adamo, J. Jaramillo, R. Gomperts, R. E. Stratmann, O. Yazyev, A. J. Austin, R. Cammi, C. Pomelli, J. W. Ochterski, R. L. Martin, K. Morokuma, V. G. Zakrzewski, G. A. Voth, P. Salvador, J. J. Dannenberg, S. Dapprich, A. D. Daniels, Ö. Farkas, J. B. Foresman, J. V. Ortiz, J. Cioslowski, D. J. Fox, *Gaussian 09, Revision D.01*, Gaussian, Inc., Wallingford CT, **2013**.
[31] R. McWeeny, *Phys. Rev.* **1962**, *126*, 1028.
[32] R. Ditchfield, *Mol. Phys.* **1974**, *27*, 789–807.
[33] K. Wolinski, A. J. Sadlej, *Mol. Phys.* **1980**, *41*, 1419–1430.
[34] K. Wolinski, J. F. Hinton, P. Pulay, *J. Am. Chem. Soc.* **1990**, *112*, 8251–8260.
[35] S. Durben, T. Baumgartner, *Inorg. Chem.* **2011**, *50*, 6823–6836.
[36] T. Agou, J. Kobayashi, T. Kawashima, *Org. Lett.* **2005**, *7*, 4373–4376.

Received: June 5, 2019